NMR study of xenon dynamics and energetics in Na–A zeolite ☆

R.G. Larsen, J. Shore, K. Schmidt-Rohr, L. Emsley, H. Long, A. Pines [1]
Materials Sciences Division, Lawrence Berkeley Laboratory, University of California, Berkeley, CA 94720, USA and Department of Chemistry, University of California, Berkeley, CA 94720, USA

M. Janicke and B.F. Chmelka
Department of Chemical and Nuclear Engineering, University of California, Santa Barbara, CA 93106, USA

Received 18 June 1993

For xenon atoms adsorbed in Na–A zeolite, electronic interactions cause shifts in NMR frequencies, resulting in a spectrum with discrete peaks from xenon atoms in cages with different xenon occupancies. Using two-dimensional exchange NMR, it is possible to determine the microscopic rates of intercage motion and to relate them to the adsorption and activation energies of the xenon atoms. The dependence of the adsorption energies on xenon cage occupancy reflects the importance of the intracage interactions and is directly related to the cage occupancy distribution. Variable temperature measurements yield an activation energy of about 60 kJ/mol for the transfer of a xenon from one cage to another.

1. Introduction

Recently, it was reported that ^{129}Xe nuclear magnetic resonance (NMR) spectra of xenon adsorbed on zeolite Na–A can be used to determine the distribution of xenon atoms among the α-cages of the zeolite [1–3]. These studies exploit the resolved resonances produced from chemical shift differences of xenon atoms in cages with different xenon occupancies, as shown in fig. 1a. Such spectra have previously been used to study the statistics of cage-occupancy [2–4]. In this Letter, we demonstrate the use of ^{129}Xe two-dimensional (2D) exchange NMR to detect magnetization exchange between the resolved resonances allowing the characterization of the intercage xenon exchange dynamics. Analysis of the intensities and rates extracted from the exchange spectra yields the change of the xenon adsorption energy as a function of cage-occupancy. Related experiments using saturation transfer NMR are under way in the laboratory of Jameson et al. [5].

The structure of dehydrated Na–A, $Na_{12}[(AlO_2)_{12}(SiO_2)_{12}]$, is known from X-ray diffraction studies to be composed of a three-dimensional array of large α-cages and smaller β-cages, with inner diameters of approximately 11.4 and 6.6 Å, respectively [6]. Each α-cage adjoins an octahedral arrangement of six other α-cages. Although sodium ions partially block the windows between adjacent α-cages, reducing the effective aperture to approximately 4.2 Å, previous studies have shown that at elevated temperatures and pressures the nominal 4.4 Å xenon atoms are readily distributed among the α-cages of micron-size Na–A zeolite crystallites [1–3]. Simple statistical models, which neglect energetics, have been shown to reproduce the general trends of the xenon distributions, observed by NMR, as a function of xenon loading [2,3]. However, systematic deviations between these models and the measured distributions indicate that energetics are significant. This is especially evident at high xenon loadings where repulsive forces are expected to be appreciable.

Average energies for a given xenon occupancy have been obtained from Monte Carlo calculations on a canonical ensemble [7–9]. The cage-occupancy dis-

[1] To whom correspondence should be addressed.

☆ Presented in part at the 34th Experimental Nuclear Magnetic Resonance Conference: St. Louis, Missouri, March 1993; Abstract P94, and at the American Chemical Society National Meeting: Denver, Colorado, March 1993; PHYS242.

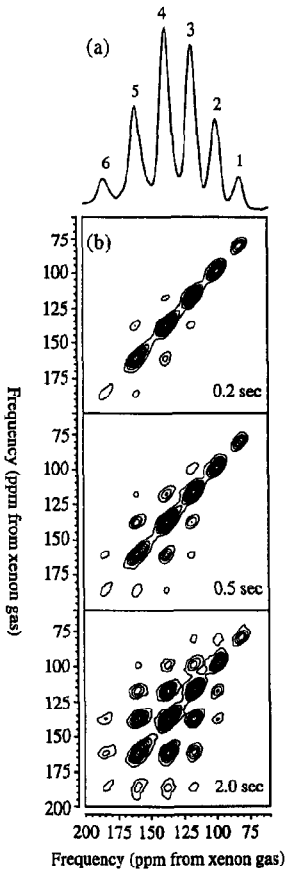

Fig. 1. (a) ^{129}Xe 1D NMR spectrum and (b) ^{129}Xe 2D exchange NMR spectra of xenon adsorbed on Na–A zeolite at 523 K and a loading pressure of 30 atm, acquired at 9.4 T (110.7 MHz) and 300 K. 2D spectra were recorded using mixing times of 0.2, 0.5 and 2.0 s. The diagonal peaks correspond to ^{129}Xe resonances from xenon in α-cages containing different numbers of occluded xenon atoms as indicated above the respective peaks of the 1D projection. The cross peaks are a result of intercage motion of xenon during the mixing time of the 2D experiment. The chemical shifts are referenced to xenon gas at low pressure.

tributions and the free energies, however, cannot be determined by this method. Though Monte Carlo calculations using a grant canonical ensemble can provide free energies and cage-occupancy distributions [10,11], so far only qualitative agreement with experiment has been obtained for the distributions [4], while free energy data have not been available. Since there exists a direct relationship between the sorbate energetics and the dynamics of intercage exchange, it is of great interest to probe the intercage motion.

The rates of both inter- and intra-cage sorbate motions can be characterized by NMR. From variable temperature measurements, McCormick and Chmelka [12] determined that at temperatures above 200 K all of the xenon atoms in a given cage appear equivalent on the time scale of the NMR experiment, due to fast intracage motion. The relatively small linewidths of the one-dimensional spectra indicate that intercage motion is slow compared to the chemical shift differences separating the resolved peaks of the spectrum ($\approx 10^3\ s^{-1}$). However, intercage xenon exchange is inferred from the observation of changes in the one-dimensional ^{129}Xe spectra over time as samples equilibrate [3]. In this Letter, we demonstrate that this slow intercage motion can be monitored directly by ^{129}Xe 2D exchange NMR in which magnetization transport during a time interval, t_{mix}, is measured. In the absence of significant spin–spin coupling between xenon atoms in different cavities, the two-dimensional spectra yield a direct measure of the mass transport of xenon between α-cages. The local energetics of xenon packing within the zeolite lattice can be determined from an analysis of the mass-transport rates.

2. Experimental

Natural-abundance xenon was distributed throughout dehydrated Na–A zeolite crystallites at xenon pressures of 5, 30, and 205 atm at 523 K, as previously described [2]. Approximately 100 Torr of oxygen was then added and the samples were flame-sealed in pyrex ampoules (10 mm outer diameter). The variable temperature measurements and most of the analysis were done using the sample prepared at 30 atm. The small amount of paramagnetic oxygen reduces the spin–lattice relaxation time of the xenon, permitting faster signal averaging. Typical recycle times were between 2 and 5 s. The ^{129}Xe NMR spectra were acquired at 9.4 T (110.7 MHz) or 11.7 T (138.3 MHz), with a Bruker AM-400 or a Chemagnetics CMX-500 spectrometer with typical $\pi/2$ pulses of 15 and 5 μs, respectively. The 2D exchange NMR spectra [13] were acquired with standard pulse sequences using TPPI [14,15] (at 9.4 T)

or the method of States et al. [16] (at 11.7 T). Typically, 64 and 256 points were acquired in t_1 and t_2, respectively, with 20 μs increments and 600 scans per t_1 value. During processing, the t_1 dimension was zero filled to 256 points and 300 Hz Gaussian linebroadening was applied in both dimensions. Xenon gas at low pressure was used as an external standard.

3. Results and analysis

^{129}Xe two-dimensional exchange NMR spectra of xenon absorbed in Na–A zeolite at 30 atm and 523 K, acquired for a range of mixing times, are displayed in fig. 1b. In such 2D spectra, the frequencies of the xenon before and after the mixing time are correlated. Denoting the frequency of an n-cage (i.e. a cage containing n xenon atoms) as $\omega^{(n)}$, the normalized spectral intensity $M(\omega^{(n)}, \omega^{(m)})$ is the joint probability of finding a xenon in an n-cage before the mixing time and in an m-cage afterwards. In the experimental spectra of fig. 1b, for the shortest mixing time (0.2 s), most of the spectral intensity is confined to the diagonal, indicating negligible intercage motion during this mixing time. For the intermediate mixing time of 0.5 s, one-off-diagonal cross peaks $M(\omega^{(n)}, \omega^{(n\pm1)})$, i.e. cross-peaks adjacent to the diagonal, at frequencies corresponding to cages differing in occupancy by one xenon, have significant intensity. This indicates that the dominant change in xenon frequencies with time corresponds to an increase or decrease of the cage occupancy by one xenon. For the spectra obtained with the longest mixing time (2.0 s), exchange is observed between all but the least populated cages. This progression of spectral features with mixing time is characteristic of mass transport in this system, and can be readily understood by considering the effect of a single-xenon intercage transfer on the ^{129}Xe 2D exchange NMR spectrum.

For the analysis of the data, it is convenient to describe the 2D peak intensities by a spectral matrix $\mathbf{M}(t_{\min})$ with $M_{n,m}(t_{\min}) = M(\omega^{(n)}, \omega^{(m)}; t_{\min})$. Approximating the magnetization transfer produced by xenon migration as a first-order process, the transfer can be described by

$$\dot{\mathbf{M}}(t_{\min}) = \mathbf{M}(t_{\min})\,\mathbf{\Pi}\,, \tag{1a}$$

with the solution

$$\mathbf{M}(t_{\min}) = \mathbf{M}(0)\exp(\mathbf{\Pi} t_{\min})\,, \tag{1b}$$

where $\mathbf{\Pi}$ is the magnetization exchange (rate coefficient) matrix. $M_{n,m}(0) = nP(n)\delta_{n,m}$ is the diagonal spectrum without exchange and exhibits spectral intensities proportional to those of the 1D spectrum. From the measured cross-peak intensities $M_{n,m}(t_{\min})$, the rate constants $\Pi_{n,m}$ can be obtained by solving eq. (1b) for $\mathbf{\Pi}$ via numeric diagonalization of $\mathbf{M}^{-1/2}(0)\mathbf{M}(t_{\min})\mathbf{M}^{-1/2}(0)$ [17,18]. It is the purpose of the following section to relate the $\mathbf{\Pi}$ matrix elements to the microscopic xenon transfer rates.

3.1. Xenon NMR kinetics

The migration of a single xenon from an α-cage with a population of n xenon atoms to an α-cage with m can result in up to three distinct cross peaks, as illustrated in fig. 2. Since the xenon resonance frequencies ω_n are sensitive to the xenon cage occupancy, the transport of a single *active* xenon atom not only can alter the frequency of the active xenon atom that was transferred, but also changes the fre-

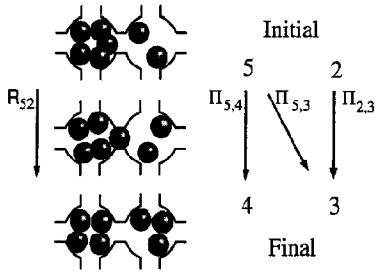

Fig. 2. Schematic representation of the relationship between the mass transport rate, $R_{5,2}$ and the magnetization transport rates $\Pi_{5,4}$, $\Pi_{5,3}$, and $\Pi_{2,3}$ for a single xenon intercage exchange event between Na–A α-cages containing 2 and 5 xenon atoms initially. Because the ^{129}Xe NMR resonance frequency of a xenon atom occluded in Na–A zeolite depends on the number of xenon in the same α-cages, three cross peaks potentially result for each intercage xenon exchange event: (1) from the active xenon atom that changes cage, (2) from the passive xenon remaining in the cage that has lost the active xenon atom, and (3) from the passive xenon in the cage that gains the active xenon atom. The magnetization transport rates are weighted by the number of xenon atoms that experience the change. Hence, for the example schematically represented the contributions to the exchange matrix are $\Pi_{5,4} = 2\Pi_{2,3} = 4\Pi_{5,3}$.

quency of *passive* xenon atoms, which undergo no intercage motion themselves but reside in cages that gain or lose an active xenon atom. In the ^{129}Xe 2D exchange spectrum, the intensity contributions from the passive xenon atoms dominate the cross peaks for two reasons: first, a single active xenon changes the frequency of $n-1+m$ passive xenons; second, while the intensities of the active xenons are distributed over all accessible frequencies $(\omega^{(n)}, \omega^{(m+1)})$, the intensities of passive xenons are concentrated in the one-off-diagonal cross peaks at $(\omega^{(n)}, \omega^{(n-1)})$ and $(\omega^{(m)}, \omega^{(m+1)})$. In other words, the NMR frequency change of the passive xenons is independent of the destination or the origin of the active xenon, so that contributions of the passive xenon atoms accumulate in the one-off-diagonal cross peaks, which dominate the exchange intensity for short mixing times. The passive xenon atoms contribute to the cross peaks farther off the diagonal via multistep exchange processes that occur during longer mixing times.

For a complete analysis, all transfer mechanisms and the corresponding rates must be considered. We define $R_{n,m}$ as the overall rate of xenon atoms going from any n-cage to any m-cage; explicit expressions for $R_{n,m}$ in terms of microscopic rates are given below. Note that the indices n and m refer to the occupancies before the transition of the xenon, so the xenon ends up in an $(m+1)$-cage and leaves an $(n-1)$-cage behind.

Due to the peculiar nature of the frequency changes generated by the xenon intercage motion, the xenon-exchange matrix elements $R_{n,m}$ are not equal to the joint-probability magnetization-exchange matrix elements $nP(n)\Pi_{n,m}$. Relationships between xenon-exchange and magnetization-exchange rates are obtained on the basis of the mechanisms discussed above and schematically represented in fig. 2,

$$nP(n)\Pi_{n,m} = R_{n,m-1}, \quad |n-m| > 1, \tag{2a}$$

$$nP(n)\Pi_{n,n-1} = \sum_{m=0}^{K-1} (n-1)R_{n,m} + R_{n,n-2}, \tag{2b}$$

$$nP(n)\Pi_{n,n+1} = \sum_{m=1}^{K} nR_{m,n} + R_{n,n}. \tag{2c}$$

While eq. (2a) and the last terms of both eqs. (2b) and (2c) describe the effects of the active xenon atoms, the dominating sum terms in eqs. (2b) and (2c) are due to the passive xenon atoms.

At equilibrium, detailed balance of the mass transport requires that

$$R_{n,m} = R_{m+1,n-1} \quad \text{and}$$

$$nP(n)\Pi_{n,m} = mP(m)\Pi_{m,n} \tag{3}$$

assuring the symmetry of the 2D spectrum.

If a statistical distribution without occupancy correlations is assumed, the rate $R_{n,m}$ is proportional to the number n of xenons in an n-cage, to the probability $P(n)P(m)$ of finding an n-cage next to an m-cage, and to the rate coefficient k_n of a given xenon leaving an n-cage,

$$R_{n,m} = nP(n)P(m)k_n. \tag{4}$$

Usually, the microscopic rate coefficient k_n is taken to exhibit an Arrhenius form $k_n = A_n \exp\{[-E_a(n)]/kT\}$ with an activation energy $E_a(n)$ and preexponential rate factor A_n.

Fig. 3a displays k_n, as a function of cage occupancy n, obtained from χ^2 fitting of all the intensities of the experimental ^{129}Xe 2D spectra measured with various mixing times (0.2, 0.5, 1.0, and 2.0 s; cf. fig. 1). The observed increase in the microscopic rates with loading can be attributed to a corresponding decrease in sorption energy, as discussed in section 3.2. The results presented in fig. 3a agree with those obtained from an analysis using the simple expression

$$\Pi_{n,n-1} \approx (n-1)k_n \tag{5}$$

obtained by combining the relations defined in eqs. (2) and (4) between $\Pi_{n,m}$, $R_{n,m}$, and k_n rate coefficients, neglecting the small term in eqs. (2b) and (2c) associated with the active xenon atoms.

3.2. Grand-canonical analysis

Xenon atoms adsorbed in zeolite cages and in thermodynamic equilibrium with xenon gas represent a grand-canonical system that can be treated in the corresponding thermodynamic terms [19]; this approach is also the basis of Monte Carlo simulations of xenon in zeolites. The grand-canonical partition function Ξ,

$$\Xi = \sum_n \lambda^n Q_n, \tag{6}$$

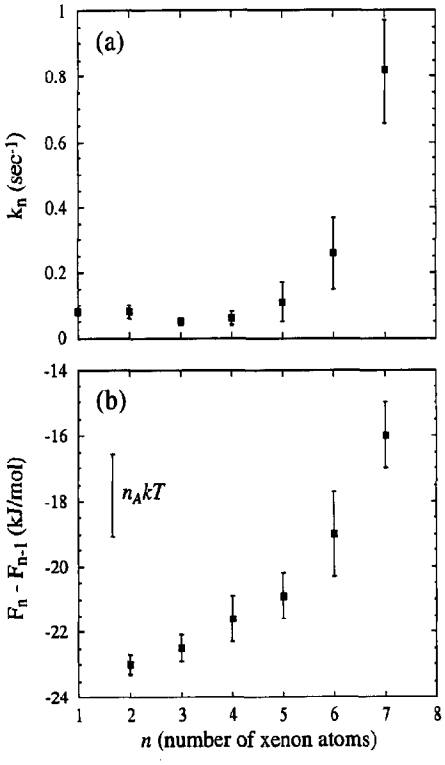

Fig. 3. (a) Xenon transfer rate coefficients, k_n, and (b) separation energies ΔF_n plotted as a function of xenon α-cage occupancy, n. The data were determined from room temperature ^{129}Xe 2D NMR spectra acquired at 9.4 T using the sample prepared at 523 K and 30 atm xenon pressure. The constant ΔF_1 is set to −23 kJ/mol [20].

is the sum over the grand-canonical distribution function $P_\Xi(n)$,

$$P_\Xi(n)=\lambda^n \frac{Q_n}{\Xi}, \tag{7}$$

with the activity $\lambda=\exp(\mu/kT)$, where μ is the chemical potential. The effects of xenon–zeolite and xenon–xenon interactions are contained in the configurational partition functions Q_n for single α-cages, which are related to the free energy F_n of the n xenon atoms in a given NaA α-cage according to

$$F_n=-kT\ln Q_n . \tag{8}$$

The relation between the xenon exchange rates $R_{n,m}$ (cf. eq. (4)) and the free energies F_n is obtained from detailed balance $R_{n,m}=R_{m+1,n-1}$. Expressing $R_{n,0}$ and $R_{1,n-1}$ according to eq. (4) using $P_\Xi(n)$ of eq. (7), one obtains rate expressions which take a general Arrhenius form

$$k_n=\frac{A}{n}\exp\left(-\frac{E^*+F_{n-1}-F_n}{kT}\right) \tag{9}$$

if Arrhenius behavior for a single xenon atom is assumed. In eq. (9), E^* denotes the energy of a xenon atom in the activated state of the transition out of an α-cage.

Defining separation energies $\Delta F_n=F_n-F_{n-1}$, according to eqs. (5) and (9) the ratios of the largest exchange-matrix elements are given by

$$\frac{\Pi_{n,n-1}}{\Pi_{m,m-1}}\approx\frac{m(n-1)}{n(m-1)}\exp\left(\frac{\Delta F_n-\Delta F_m}{kT}\right). \tag{10}$$

The separation energies, obtained through this relation from the experimental ^{129}Xe 2D exchange spectra and refined by χ^2 fitting of the complete set of 2D intensities, are plotted in fig. 3b. The constant ΔF_1 is set to −23 kJ/mol [20], taken from adsorption measurements at very low xenon concentrations. The observed decrease in the absolute values of the separation energies $|\Delta F_n|$ at loadings of $n>5$ can be attributed to crowding of the xenon in the α-cages and results in the absence of NMR signals, for our samples, from xenon in cages with occupancies of eight or higher.

In fig. 4 we show the experimental and simulated ^{129}Xe 2D NMR spectrum of xenon adsorbed on NaA zeolite. The simulated spectrum was produced using the separation energies of fig. 3b and a first-order rate coefficient (k_1) of 0.09 s^{-1}. The relatively rapid increase of cross-peak intensity with mixing time for the higher occupancies is a direct result of the occupancy dependence of the adsorption energies. Further measurements of this sample at 336 and 357 K yield a preliminary estimate of E^*-F_1 of 60 kJ/mol and a preexponential factor of 10^{10} s^{-1}.

Analysis of many 2D exchange data sets measured on different samples reveals a systematic mixing-time-dependent deviation from the exchange kinetics described above, which can be described as an apparent slowing down of the dynamics. It is not due to the deviation of the actual xenon exchange process from first-order kinetics, since this would give rise to a much smaller effect as predicted using sim-

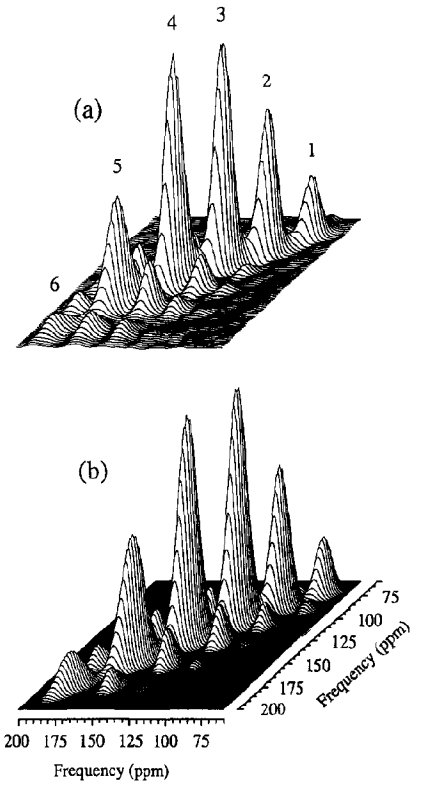

Fig. 4. ^{129}Xe 2D exchange NMR (a) spectrum and (b) simulated spectrum of xenon adsorbed on Na–A zeolite. The sample was prepared at 523 K and 30 atm xenon pressure. The spectrum was acquired at 9.4 T (110.7 MHz) and 300 K with a mixing time of 0.5 s. The numbers represent the number of xenon atoms in the α-cage of the corresponding diagonal peak. The simulation (b) employs the separation energies (cf. fig. 3) determined from the full set of experimental spectra taken at this temperature.

ple Monte Carlo simulations. The effect also cannot be explained by incomplete equilibration of xenon within a given crystallite, because it was also observed in samples which have had several years to equilibrate. The apparent slowing down of the kinetics with increasing mixing time could be due to a distribution of activation energies, and may involve a distribution of cage sorption energies or of activated state (window) energies. The latter appears more probable, since heterogeneity in terms of window occlusion is more easily imagined than differences in the structure of the individual cages. Further higher-dimensional exchange NMR experiments should permit clarification of the nature of the nonexponentiality [21].

The 2D experiments show that the xenon distributions in zeolite Na–A equilibrate at room temperature by intercage exchange. As a consequence of these equilibration processes, the distributions reflected in ambient-temperature spectra do not represent "frozen" high-temperature distributions, unless the measurements are performed within a few hours after the sample preparation.

Finally, we note that the 2D experiment measures intercage xenon transfer processes, which are the elementary steps for diffusion of the sorbed xenon in the zeolite crystallites. Using the microscopic rate coefficients k and the relation $D=k\,(1.14\ \mathrm{nm})^2$ we can estimate the diffusivity to be 0.1 $\mathrm{nm^2/s}=10^{-19}$ $\mathrm{m^2/s}$ at ambient temperature, which is much smaller than the values accessible by pulsed field gradient techniques [22]. It should be noted that exchange rates of the order of 0.1 $\mathrm{s^{-1}}$ can be easily measured using mixing times of 1 s or less due to the enhancement of the cross peaks by the passive xenon atoms.

4. Conclusions

Using ^{129}Xe 2D exchange NMR, we have measured the magnetization transport rates, determined the corresponding mass-transport rates, and from this obtained relative xenon adsorption separation energies, as a function of xenon cage occupancy in NaA zeolite. The separation energies are relatively constant up to an occupancy of four xenons in a cage. For higher occupancies, the separation energies are decreased by several RT due to repulsive interactions as the cages become more crowded. From variable temperature measurements, we have estimated the activation energy required for a xenon atom to move from one cage to another. Other questions to be addressed using the same technique and analysis include the effects of co-adsorbates, both in relation to the distribution as well as to the dynamics of the xenon, co-adsorbed species and cations. Furthermore, if all the xenon rates are measured, it should also be possible to determine pair correlations of cage occupancies.

Acknowledgement

This work was supported by the Director, Office of Energy Research, Office of Basic Energy Sciences, Materials Sciences Division of the US Department of Energy under Contract No. DE-AC03-76SF00098, and also by a grant from the Shell Development Company. LE is a fellow of the Miller Institute for Basic Research in Science. KSR thanks the BASF AG and the Studienstiftung des deutschen Volkes for a fellowship. BFC acknowledges funding support through the NSF Young Investigator program under grant DMR-9257064 and from the Camille and Henry Dreyfus Foundation.

References

[1] M.G. Samant, L.C. de Ménorval, R.A. Dalla Betta and M. Boudart, J. Phys. Chem. 92 (1988) 3937.
[2] B.F. Chmelka, D. Raftery, A.V. McCormick, L.C. de Menorval, R.D. Levine and A. Pines, Phys. Rev. Letters 66 (1991) 580.
[3] C.J. Jameson, A.K. Jameson, R. Gerald II and A.C. de Dios, J. Chem. Phys. 96 (1992) 1676.
[4] P.R. VanTassel, H.T. Davis and A.V. McCormick, J. Chem. Phys., in press.
[5] A.K. Jameson, C.J. Jameson and R.E. Gerald II, Presented at the American Chemical Society National Meeting: Denver, Colorado, March 1993; PHYS241.
[6] J.J. Pluth and J.V. Smith, J. Am. Chem. Soc. 102 (1980) 4704.
[7] P.R. VanTassel, H.T. Davis and A.V. McCormick, Mol. Phys. 73 (1991) 1107.
[8] P.R. VanTassel, H.T. Davis and A.V. McCormick, Mol. Phys. 76 (1992) 411.
[9] P.R. VanTassel, C. Hall, H.T. Davis and A.V. McCormick, Pure Appl. Chem. 64 (1993) 1629.
[10] G.B. Woods, A.Z. Panagiotopoulos and J.S. Rowlinson, Mol. Phys. 63 (1988) 49.
[11] G.B. Woods and J.S. Rowlinson, J. Chem. Soc. Faraday Trans. II 85 (1989) 765.
[12] A.V. McCormick and B.F. Chmelka, Mol. Phys. 73 (1991) 603.
[13] J. Jeener, B.H. Meier, P. Bachmann and R.R. Ernst, J. Chem. Phys. 71 (1979) 4546.
[14] G. Drobny, A. Pines, S. Sinton, D.P. Weitekamp and D. Wemmer, Faraday Symp. Chem. Soc. 13 (1979) 49.
[15] G. Bodenhausen, R.L. Vold and R.R. Vold, J. Magn. Reson. 37 (1980) 93.
[16] D.J. States, R.A. Haberkorn and D.J. Ruben, J. Magn. Reson. 48 (1982) 286.
[17] E.W. Abel, T.P.J. Coston, K.G. Orrell, V. Sik and D. Stephenson, J. Magn. Reson. 70 (1986) 34.
[18] C.L. Perin and T.J. Dwyer, Chem. Rev. 90 (1990) 935.
[19] D.A. McQuarrie, Statistical mechanics (Harper and Row, New York, 1976).
[20] D.M. Ruthven, Principles of adsorption and adsorption processes (Wiley, New York, 1984).
[21] K. Schmidt-Rohr and H.W. Spiess, Phys. Rev. Letters 66 (1991) 3020.
[22] J. Karger and H. Pfeifer, Zeolites 7 (1987) 90.